

Understanding the chemistry of cation leaching in illite/water interfacial system using reactive molecular dynamics simulations and hydrothermal experiments

Murali Gopal Muraleedharan,^a Ryan Herz-Thyhsen,^b Janet C. Dewey,^b John P. Kaszuba,^{b,c} and Adri C. T. van Duin^a

^aDepartment of Mechanical Engineering, The Pennsylvania State University, University Park, PA 16802, United States

^bDepartment of Geology and Geophysics, University of Wyoming, 1000 E. University Avenue, Laramie, Wyoming 82071, United States

^cSchool of Energy Resources, University of Wyoming, 1000 E. University Avenue, Laramie, Wyoming 82071, United States

Abstract

Despite long standing pursuit, fundamental questions concerning the chemical pathways of leaching of ions in minerals, a phenomenon crucial to energy extraction, hydrometallurgy, metal recovery, and agriculture remain unanswered. Here we use large-scale ReaxFF reactive molecular dynamics (MD) simulations in combination with hydrothermal experiments to understand the chemistry of leaching in illite exposed to aqueous environment. Our simulations show that potassium counterions leach out into the solution much earlier and in higher concentration when compared with aluminum and silicon, which form the structural network of illite. Upon analyzing the chemical pathway from the trajectory of MD simulations, water molecules supply protons near the illite surface that binds with the non-bridging oxygen (NBO) of the Al-O-Si linkage forming an [Al-O-Si]---H transition state that later converts to silanol group upon Al-O bond dissociation. Proton addition also weakens the interlayer K-O bonds, resulting in the diffusion of K⁺ ions to illite surface, where they combine with the hydroxyl group formed from water dissociation, to form KOH molecules. KOH molecules diffuse out reactively to bulk water via proton exchange mechanism. Furthermore, we also find that continued protonation results in the formation of Al(OH)₃ and Si(OH)₄ groups predominantly at the surface, which diffuse out into water resulting in the leaching of Al and Si cations. We also estimated the kinetics of surface reactivity from the MD simulations and explored its effectiveness as a surrogate model for leaching kinetics. However, surface reaction kinetics and experimentally measured leaching kinetics seemed to be off by several orders of magnitude. We also analyzed the effects of leaching on structural distortion and found that more than 20% leaching is required for a notable structural distortion in illite crystal.

1. Introduction

Revolutionary transformations in environmentally friendly and sustainable technologies for carbon capture and sequestration, energy recovery and storage, membranes for air and water purification, and catalysis can be achieved through a molecular-level understanding of interactions of fluids at solid surfaces. One such fluid-solid interaction significant to myriad scientific applications is leaching.[1] Despite persistent efforts, fundamental questions concerning the chemistry of leaching remain unanswered.

Leaching is the process by which cations from solids are released to surrounding fluid (leachate) when the solid and fluid are placed in contact with each other for a period of time. Leaching is relevant to numerous engineering applications: energy extraction,[2–4] hydrometallurgy,[5–7] metal recovery,[8,9] agriculture,[10–12] etc. In energy extraction from unconventional petroleum reservoirs, injection of fluids during hydraulic fracturing may induce cation leaching resulting in dissolution of minerals surrounding fractures. This can result in structural and morphological changes in the minerals that can have effects on hydrocarbon mobility through the fractures[13,14]. In hydrometallurgy and metal recovery, targeted cations can be leached from ores or worn-out batteries and devices by dissolving them in chemically treated water[15]. Likewise, in agriculture, water is used to release minerals from the soil to water that can be mobilized and made accessible to plants[10].

Leaching can occur in acidic, alkaline, or neutral environments. In an acidic medium, the acid supplies protons that bind with the solid and removes cations which eventually leach out. Applications of acid leaching include extraction of copper from oxide- or sulfide-bearing ore and dissolution of uranium from sandstone ores.[16,17] If an alkaline medium is used, hydroxyl groups supplied by the alkali bind directly with metal cations and eventually leach them out. For example,

sodium hydroxide can be used for dissolving aluminum from bauxite and leaching wolframite and scheelite ores,[18] and ammonium hydroxide can be used for extracting metals such as copper and nickel that form soluble ammines from their ores.[19] Often times, a neutral solution (typically water) is chosen as the leachate as opposed to acids or alkalis to facilitate an environmentally friendly leaching process. The removal of metal cations could be carried out either by protons or hydroxyl groups depending on the local pH value, chemical environment, and reaction energy barriers. Leaching, therefore, needs to be methodically studied to enable the design of appropriate solid-fluid combinations to address pressing technological challenges of energy sustainability.

Interaction of natural materials like clays and ceramics with fluids gives us reliable and relatively inexpensive avenues to understand the chemistry of leaching. Hence, in this work, we study the chemistry behind leaching and subsequent structural transformations on illite in contact with water. Illite is a clay mineral; a common component of unconventional reservoirs.[20] Unconventional reservoirs commonly occurring in low-permeability rocks necessitates the use of hydraulic fracturing to artificially create avenues for fluid flow, requiring injection of large volumes of chemically-treated water. After contact with the water, leaching of K, Al, and Si cations from illite present in the rock can result in structural and morphological changes to the rock. Since illite dissolution occurs on timescales comparable to that of the hydrocarbon production, changes in rock properties surrounding fractures may alter fluid mobility through the rock.[21] Hence from a practical point of view too, this study would enable one to design efficient hydraulic fracturing fluids, enabling hydrocarbon flow from subsurface in an environmentally friendly manner.

The ideal approach to elucidate leaching mechanism is by collecting different mineral samples from subsurface rocks and placing them in contact with fluid to gain insights from hydrothermal experiments. However, leaching of metal cations from clay minerals when in contact with water

is a relatively slow process as the proton concentration tends to be low and hence can take several months to achieve solubility equilibrium. Furthermore, it is also challenging to study the chemical reactions that lead to leaching as naturally obtained clays are a mixture of different types of minerals: illite, kaolinite, smectite, etc. In such situations, it will be of great utility to have an experimentally benchmarked predictive model for cation leaching in such situations. Numerical simulation techniques like Monte Carlo (MC) methods,[22–24] Molecular Dynamics (MD),[25–27] and Density Functional Theory (DFT)[28,29] have been applied to clay hydration problems in the past as attempts to investigate water dynamics on clay surfaces. In these cases, however, addressing the relevant surface chemistry has indeed been a challenge, as the surface modification is coupled to hydration, and the resulting surface chemistry is dynamic on a timescale one tries to characterize the surface. To yield relevant physical insights in such cases, atomistic simulations like ReaxFF reactive molecular dynamics [30,31] methodology have been proven to be useful.

ReaxFF is an attractive approach in predicting the dynamics of cation leaching as it can capture the chemical reactions leading to mineral dissolution. ReaxFF also allows the user to deterministically set up an initial geometry constituted by an initial atomic composition and arrangement, and then rely on the reaction-diffusion processes to drive the system towards local chemical equilibria. This feature is much more general compared with a non-reactive MD simulation using an empirical potential where the system topology remains constant throughout the simulation. Moreover, recent advancements in MD simulations have been able to scale up the system size to as many as several million atoms[32–34] efficiently while still retaining near-quantum mechanical accuracy, especially for reaction barriers and enthalpies. For these reasons, ReaxFF has been used in the past to simulate the dynamics of water in contact with inorganic materials.[33,35,36] For instance, recent work by Hahn and van Duin[35] simulated the leaching

of sodium cations from amorphous sodium silicate glass in aqueous environment using a forcefield developed for Na/Si/O/H systems[37]. In their study, at ambient conditions, they observe a substantial amount of Na⁺ cations leaching into water in the form of NaOH molecules. However, they do not report the dissolution of Si⁴⁺ cations as the Si-O-Si structure was observed to be stable at ambient conditions. They also elucidate the mechanism of leaching through a statistical analysis of the MD trajectory.

The primary goal of this work is to leverage the capabilities of ReaxFF to model and simulate a rather challenging and long-timescale chemical process and elucidate the chemistry of illite dissolution when exposed to water. We first implement ReaxFF/MD to study the mechanism of leaching of K, Al, and Si cations. The energy barriers of important reactions are also evaluated to ascertain why the leaching sequence follows a certain order. Next, the solute concentrations are quantified and used to determine the early stage reaction kinetics. Then we conduct hydrothermal experiments on illite-containing rocks in contact with water until the solution saturates (216 days). By comparing the reaction kinetics from MD and experiments, we reveal the shortcomings of surface reaction kinetics in predicting leaching kinetics. Finally, leaching-induced structural transformations in illite crystal is also investigated.

2. Materials and Methods

2.1. ReaxFF Reactive MD simulations

ReaxFF is a bond-order dependent potential, wherein the total energy of the system consists of contributions from bond-order dependent terms and non-bonded interaction terms. The connectivity between all atom pairs is calculated on-the-fly from the local atomic environment and updated every time step of the simulation. This feature allows ReaxFF to capture the chemical

reaction process systematically. Bond-order is calculated based on the interatomic distances of all atom pairs in every time step. Therefore, the energy contributions from bond-order dependent terms such as bond, valence angle, and torsion angle disappear upon bond dissociation, and only the non-bonded interactions such as van der Waals and Coulombic energies need to be considered thereafter. Atomic charges required to calculate the non-bonded interaction energies is a dynamic quantity, is derived using the electronegativity equalization method (EEM)[38]. More details on the ReaxFF functional form and implementation can be found in Ref.[31]

To describe the atomic interactions in water, we used the H/O parameters trained against training sets obtained via DFT calculations containing geometries of water clusters with 2-35 water molecules, proton transfer barriers in these clusters, bond dissociation energies of H₂O, O₂, and H₂, proton transfer reactions in OH/H₂O and H₃O⁺/H₂O clusters, angular distortions, vibrational frequencies, and equation of state of crystalline ice. The H/O parameters have been successfully implemented in prior reactive MD studies for simulating interaction of water with clay minerals smectite and zeolite[33]. For this work we combined the H/O/Si/Al[33] with the H/O/K [34] description to obtain a transferable H/O/Si/Al/K force field for clay minerals containing potassium counterions. The interaction parameters were originally optimized by training against the solvation energies of various cations and radicals in water, bond lengths and bond angles of the various conformations of the cation/water clusters, water binding energies of the aforementioned clusters, equations of state for the condensed metal, metal oxide, and metal hydroxide, and the heats of formation for metal oxide and metal hydroxide phases from elemental states. Training set data were obtained via density functional theory calculations or from experimental data in the literature.[33,34]. Note that this forcefield strictly describes only K⁺ ions in water and K⁺ bound to

Al/O/Si surfaces, similar to the previously reported Na/Si/O/H forcefield[37] but not K/Al/Si/O/H bulk phases.

2.1.1. Simulation geometry

Illite is a dioctahedral phyllosilicate with a 2:1 arrangement of tetrahedral silicate and octahedral aluminum layers. The space between the TOT layers have trapped potassium cations constituting a T-O-T (K⁺) T-O-T structure. We prepared the illite sheet by stacking unit cells of crystallographic directions. The crystalline illite structure used for the simulations, hence, consisted of 10 x 10 x 2 unit cells with lattice parameters $a = 5.22 \text{ \AA}$, $b = 9.02 \text{ \AA}$, and $c = 10.07 \text{ \AA}$. This structure was first independently energy minimized with the (001) cleavage plane intentionally exposed to vacuum and leveraging the reactive forcefield for surface atomic rearrangements and optimization. Following this, the system is equilibrated at $T = 298 \text{ K}$ and $P = 1 \text{ bar}$ with periodic boundary conditions but leaving 2 \AA of vacuum on either side of the free surface.

Single water molecules were independently created based on the geometric parameters: O-H bond length = 1 \AA , and H-O-H bond angle = 104.5° and allowed to relax to lowest energy configuration within the reactive force field. The number of water molecules were decided on the basis of the chosen temperature and pressure, and water molecules were randomly added to the system until the desired density was achieved. Thereafter the water system was independently energy minimized and equilibrated at target temperature and pressure.

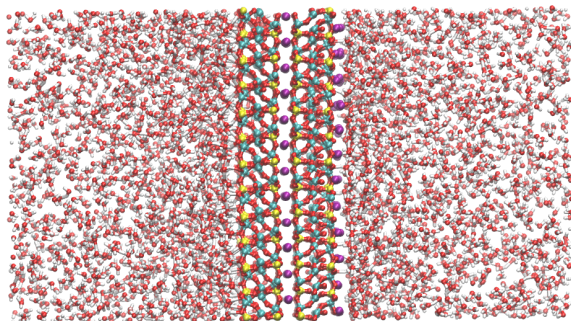


Figure 1. Simulation domain consisting of illite structure with water on either side at $T=2000$ K and $P=100$ MPa, consisting of 14352 atoms. Color legend: O (Red), H (White), Si (Blue), Al (Yellow), K (Purple).

The independently equilibrated water and illite structures were then combined to form an interface as shown in Fig.1. Figure 1 is representative of the system at $P=100$ MPa and $T=2000$ K with water on either side of the illite structure allowing sufficient surface area for protonation and avenues for other surface reactions that can potentially lead to leaching events.

2.1.2. Simulation settings

We used ReaxFF integrated into the Amsterdam Density Functional (ADF) [39] for reactive MD simulations. All simulations were run in the canonical (NVT) ensemble using a weak Berendsen thermostat with temperature damping constant of 0.1 ps to keep the temperature constant. A time step size of 0.25 fs was used, and the equations of motion were integrated using the velocity-Verlet integration scheme.[40] For each temperature, the combined illite/water system was energy-minimized and equilibrated for 50 ps, until the total potential and kinetic energies have reached a constant mean value before starting the MD production run. We targeted elevated temperatures ($T = 2000, 2500,$ and 3000 K) to accelerate the reaction kinetics and achieve chemical reactions in timescales achievable using MD simulations. Once equilibrated, the system was run

for 0.5 ns allowing for solution to leach cations. During the simulation run, we monitored and recorded the changes in energy, system parameters, and mole fractions of various species, and later post-processed them to obtain relevant results. We performed four independent repetitions of the simulation at each temperature starting from different initial geometries and obtained the mean values to ensure an unbiased statistical sampling of the MD trajectory.

2.2. Hydrothermal experiments

To compare with reactive MD predictions, we also conducted hydrothermal experiments. Details of the experiment are described in Herz-Thyhsen et al.,[41] and the experimental information is summarized in Table 1.

Table 1. Hydrothermal experimental conditions[21]

Temperature (K)	488 ± 0.2
Pressure (MPa)	35 ± 0.2
Fluid mass (g)	302
Rock mass (g)	14.5
Fluid-rock ratio	20.1:1
Duration (days)	216

The hydrothermal experiment was performed in a rocking furnace-pressure vessel assembly using established methods [42,43]. Rock used in the experiment was cut from core of the Wall Creek Member of the Frontier Formation from the Powder River Basin, Wyoming. The rock is a calcite-cemented quartz sandstone containing accessory illite, chlorite, kaolinite, pyrite, and albite. Fresh water was combined with chemical additives to create the stimulation fluid used in the experiment. Stimulation fluid and cubes of rock were combined in a gold reaction cell at a water-rock ratio of 20:1 to emulate the volume of fluids relative to the surface area of rocks exposed in millimeter-scale fractures. [44] The cell was subsequently sealed, pressurized to 35 MPa, and

heated to 488 K. The experiment was conducted for ~5200 hours (216 days), longer than the typical amount of time (30 days) between hydraulic fracturing and the time the well is opened for fluid production. This extended timeframe was chosen because most stimulation fluid injected into the subsurface is trapped in the rock, suggesting that the stimulation fluid reacts with rock over an extended period of time.

Aqueous samples were periodically collected from the experiment to monitor reaction progress and quantify the in-situ chemical evolution of the stimulation fluid. The geochemistry of the final sample and the aqueous sample collected immediately prior to terminating the experiment were also compared to determine whether retrograde mineral reactions or mineral precipitation/dissolution may have occurred as an artifact from cooling and degassing the experiment. Cations were analyzed using inductively coupled plasma optical emission spectrometry (Perkin Elmer Optima 8300) and anions were analyzed using ion chromatography.[45] Total dissolved inorganic carbon was measured using coulometric titration [46] and ex-situ pH was measured using an Orion pH meter. In-situ pH was calculated by speciating the fluid using The Geochemist's Workbench® version 10, the b-dot ion association model, and the thermo.tdat thermodynamic database.[41]

3. Results and Discussion

3.1. Dissolution of K, Al, and Si from hydrothermal experiments

Table 2 shows the time evolution of pH and the concentration of K, Al, Si in the fluid. Note that time, $t = 0$ denotes the time at which the experimental cell was sealed, which is about 14.5 hours after the cell was assembled. The *ex situ* pH increases from an initial value of ~2.5 (the pH of the fluid) to near neutral in less than 27 h where it remained for the duration of the experiments.

The initial rise in pH may be due to the increased concentration of hydroxyl ions resulting from surface-catalyzed water splitting, meanwhile the protons chemisorb to the surface and form Al-OH and Si-OH groups.

Table 2. Time evolution of chemistry of the fluid in hydrothermal experiment

Time (h)	pH (<i>ex situ</i>)	K (mmol/kg)	Al (mmol/kg)	Si (mmol/kg)
0	2.47	1.14	0.002	0.17
6	-	0.98	0.081	1.03
26	6.68	1.92	0.011	1.24
50	6.31	1.94	0.006	1.61
121	6.40	1.76	0.006	1.92
361	6.61	1.90	0.008	2.25
865	6.57	1.63	0.003	2.82

K⁺ ions in solution shows an initially high concentration of 1.14 mmol/kg which reduces by ~10% in the first 6 h, and again increases to 1.92 mmol/kg as the experiment proceeds in time. The initially high concentration may be ascribed to the dissolution of K⁺ ions from illite surface by forming KOH molecules. As time proceeds, K⁺ ions in the interior diffuse to the surface and leach into the fluid. During the same time, KOH molecules in solution also precipitate on to the surface, which manifests as reduced concentration at 6 h and 121 h. Similarly, note that the aqueous Si concentration increases by about 10 times in the first 50 hours of the experiment and continues to increase slightly throughout the experiment. This may be credited to the formation of Si(OH)₄ molecules that eventually diffuse into bulk fluid. Aqueous Al concentration, on the other hand, increases by about 40 times in the first 6 hours which may be due to the formation and dissolution

of $\text{Al}(\text{OH})_3$, which later precipitates on to surface, indicated by the decrease in concentration beyond 50 h. [21] In the following sections, we use ReaxFF/MD to test these hypotheses and elucidate the mechanism of illite dissolution.

3.2. ReaxFF investigation of surface reactivity and leaching of cations

Before investigating chemical reactivity at the illite/water interface, we ensure that water has properly wetted the illite surface. Wetting is a non-reactive interaction, primarily due to van der Waals and Coulombic forces between the dipoles of water and the induced dipoles on the illite surface. This manifests as a marginal drop in total potential energy of the system of ~ 1 kcal/mol energy of hydration/wetting, which is comparable to the values reported in the literature[47,48]. As the surface wetting process continues, it is important to ensure a proper equilibration of the system by simultaneously monitoring the system energy and mean number density of water molecules in the region adjacent to the illite surface. Also note that wetting results in a locally denser water layer near the surface, as observed in prior MD simulations [49], setting stage for surface protonation events.

Once the surface has wetted, within a few picoseconds, reactions start to occur. The first notable reactions are the protonation of illite surface as illustrated in Fig. 2. In the protonation mechanism, water molecules weakly bind with non-bridging oxygen (NBO) of the Al-O-Si linkage forming a $[\text{Al-O-Si}] \cdots \text{H}$ transition state and a free hydroxyl ion, as shown in Fig. 2(b). Following this, the Al-O bond of the Al-O-Si linkage stretches (Fig. 2(c)) and breaks to form a silanol group (Fig. 2(d)) at the surface, leaving a terminal Al that transitions from octahedral to tetrahedral state whereas the hydroxyl remains near the surface resulting in locally higher pH values, which explains the rise in pH observed in experiments.

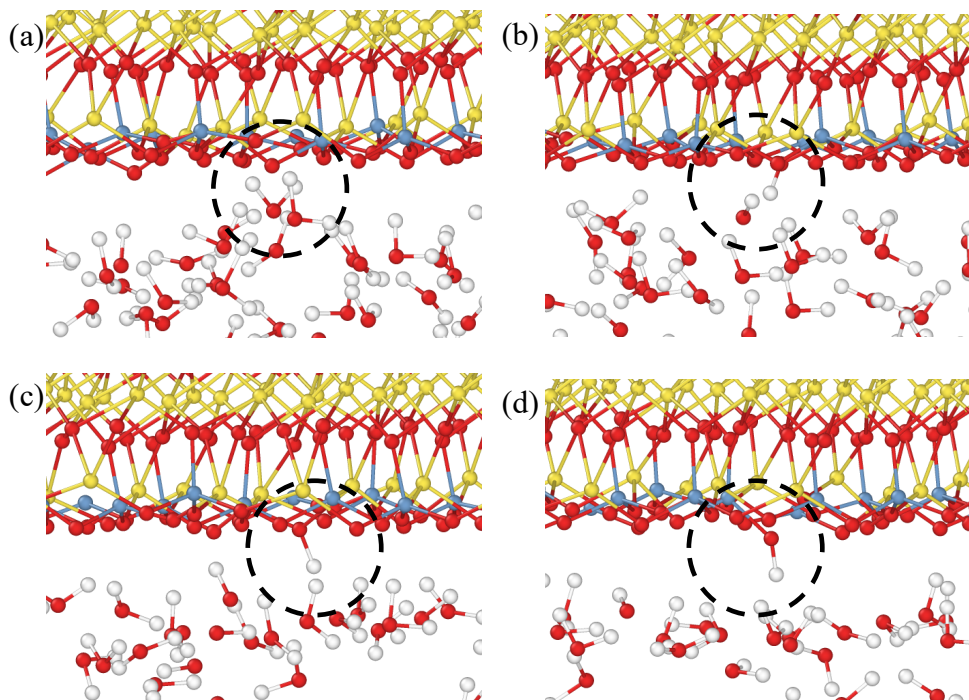


Figure 2. Protonation of the illite surface and subsequent formation of silanol groups at the surface.

a) Circled area shows the target NBO site and the water molecule targeting the NBO site, b) Proton addition to the NBO site resulting in the formation of $[Al-O-Si]---H$ transition state and a free hydroxyl radical c) Stretching of the Al-O, Si-O, and the O-H bonds resulting in the dissociation of Al-O bond of the Si-O-Al linkage d) Formation of Si-OH group at the surface

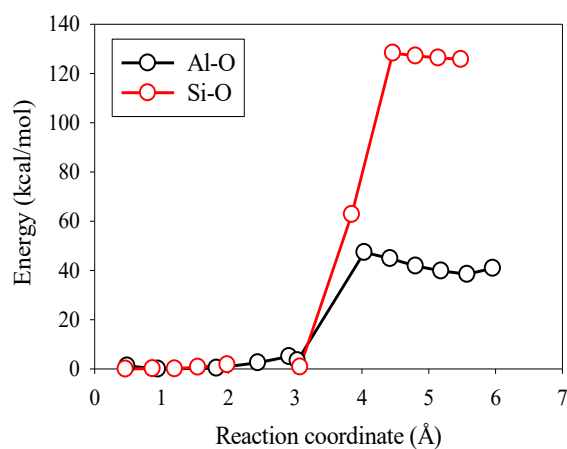


Figure 3. Evaluation of reaction energy barriers of Al-O and Si-O bond dissociation reactions using Nudged elastic band (NEB) method.

To further elucidate the Al-O bond dissociation reaction, we calculated their energy barriers by nudged elastic band (NEB) method as shown in Fig. 3. [50] In NEB, a string of geometric configurations (open circles in Fig. 3) of the system is used to describe a reaction pathway. These configurations connected by spring forces are equispaced along the reaction path. Upon convergence of the NEB to the minimum energy path, the configurations describe the reaction mechanism. Results of NEB method suggests that the dissociation energy of Al-O and Si-O bonds are 131 kcal/mol and 49 kcal/mol respectively, from which, it is evident that protonation of the surface oxygens is more likely to result in Al-O than in Si-O bond dissociation. Also note that both are endothermic reactions, and hence, favor elevated temperatures. At low temperatures, the reaction kinetics are slow and raising the system temperatures in MD simulations, therefore, helps accelerate the reaction kinetics of surface protonation for subsequent reactions.

3.2.1. Weakening of K-O bonds and formation of K-OH bonds by K⁺/H⁺ exchange

Following the formation of hydroxyl ions in dissociated water, the excess negative charge needs to be stabilized immediately by electrostatically combining a positively charged cation from the surroundings. A direct effect of surface proton addition is the weakening of inter-layer K-O bonds. K⁺ counterions have now become more mobile and diffuse through the illite structure; some of which manage to reach the surface.

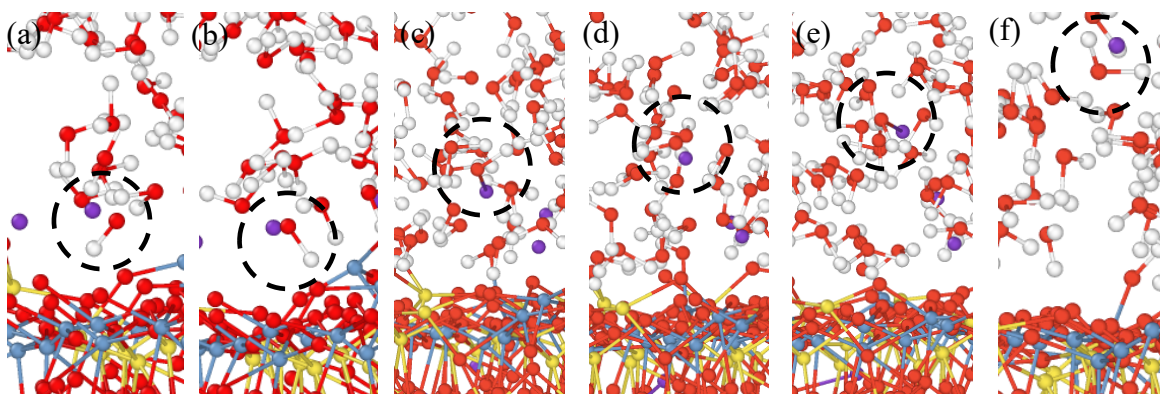


Figure 4. Sequence of events leading to formation of KOH molecules at the interfacial water layer and reactive diffusion of KOH molecule into bulk water by K^+/H^+ exchange mechanism. a) Circle showing the K^+ cation and the OH^- anion b) $K-OH$ molecule formation resulting in the neutralization of charges, c) KOH molecule in the vicinity of water molecules d) Proton hopping resulting in dehydroxylation of K^+ and OH^- e) K^+ combines with OH^- formed in (b) resulting in a 2 step K^+/H^+ exchange mechanism, f) KOH diffuses outwards by successive H^+/K^+ mechanism

At the surface, K^+ cations are exposed to surrounding water molecules and free hydroxyl ions, as shown in Fig. 4(a). Figure 4(b) shows the neutralization of hydroxyl ion by a K^+ ion resulting in the formation of a KOH molecule. We observed that the K^+ cations diffuse away from the interface into bulk water via K^+/H^+ exchange or proton hopping mechanism as illustrated in Fig. 4 (c)-(f). In the light of our observations, we define three regimes of weak K counterion leaching in clay/water interfacial systems: 1) Diffusion within the Al-O-Si structural framework, 2) Reaction with hydroxyl ions to form metal hydroxide, and 3) Reactive diffusion in bulk water by proton hopping mechanism. Hahn and van Duin [35] have also observed a similar trend in the leaching of Na^+ cations from glass surfaces.

3.2.2. Continued surface protonation and dissociation of Al-O and Si-O bonds

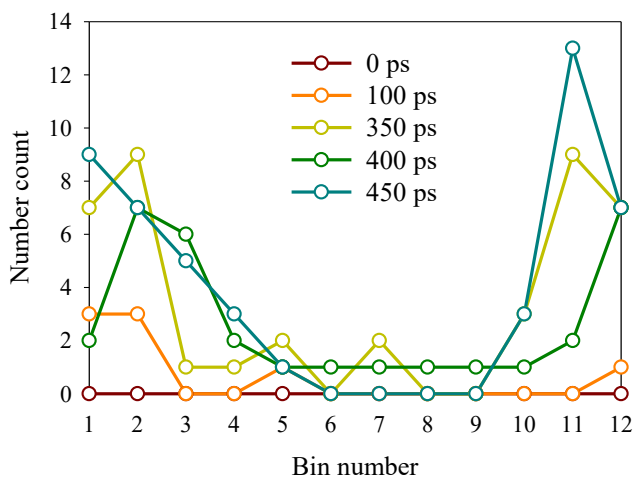


Figure 5. Proton number count inside the illite structure at different instances of the simulation run. The illite structure is divided into 12 bins and proton number count inside each bin is calculated at various times from the MD trajectory file. It is clear that the total protonation density increases with time and the proton density in the interior of illite also increases due to the diffusion of protons from surface to bulk illite. Bins 1 and 12 represent the illite surfaces.

Surface protonation continues as more water molecules traverse in and out of the interfacial layer, which is at a local protonation/deprotonation equilibrium. We calculated the number of protons in various bins along the (001) direction of the illite structure (Fig. 5). As seen in Fig. 5, surface protons diffuse into bulk solid with time. It is presumed that continued surface proton diffusion to the interior helps in leaching out cations. Al^{3+} and Si^{4+} leach out predominantly from the surface in the form of $\text{Al}(\text{OH})_3$ and $\text{Si}(\text{OH})_4$ respectively. Note that, unlike K^+ counterions, three distinct regimes of leaching cannot be identified for Al and Si because they form the illite network and Si and Al leaching events are localized to the surface. Figure 6 and 7 illustrate the

formation and dissolution of $\text{Si}(\text{OH})_4$ and $\text{Al}(\text{OH})_3$ molecules respectively from the surface to water by a combined reactive/non-reactive diffusion.

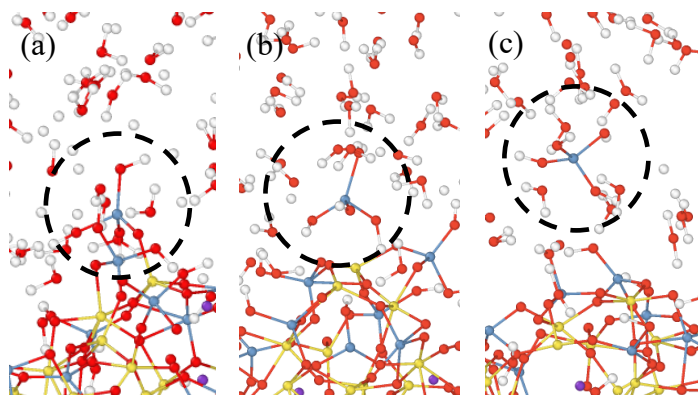


Figure 6. Formation and diffusion of $\text{Si}(\text{OH})_4$ molecule at the illite surface a) Formation of $\text{Si}(\text{OH})_4$ molecule from a surface $\text{Si}(\text{OH})_3\text{-O-Al}$ formed from continuous surface protonation b) Nascent $\text{Si}(\text{OH})_4$ molecule at the surface formed due to continuous protonation and subsequent formation of silanol groups, c) Schematic of combined reactive and non-reactive diffusion of $\text{Si}(\text{OH})_4$ to bulk water. Reactive diffusion occurs by proton exchange mechanism whereas non-reactive mechanism occurs due to density gradients.

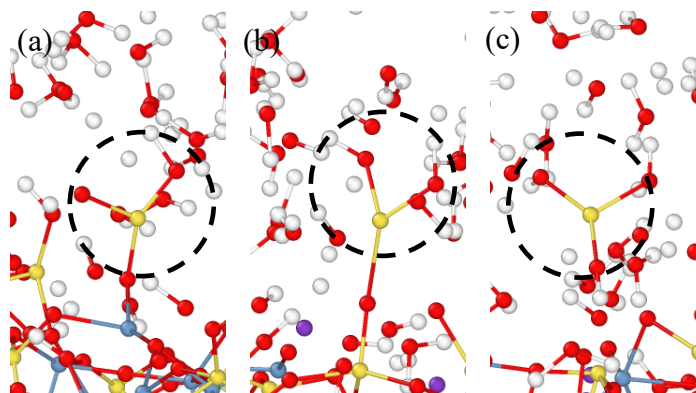


Figure 7. Formation and diffusion of $\text{Al}(\text{OH})_3$ molecule at the illite surface a) Formation of $\text{Al}(\text{OH})_2\text{-O-Si}$ at the surface b) Formation of $\text{Al}(\text{OH})_2\text{-O-Si}$ upon protonation of an unbonded O, and stretching of the Al-O bond before dissociation resulting in an undercoordinated surface Al

group that is neutralized by a hydroxyl radical, c) Nascent $\text{Al}(\text{OH})_3$ forms near the surface and diffuses out to bulk.

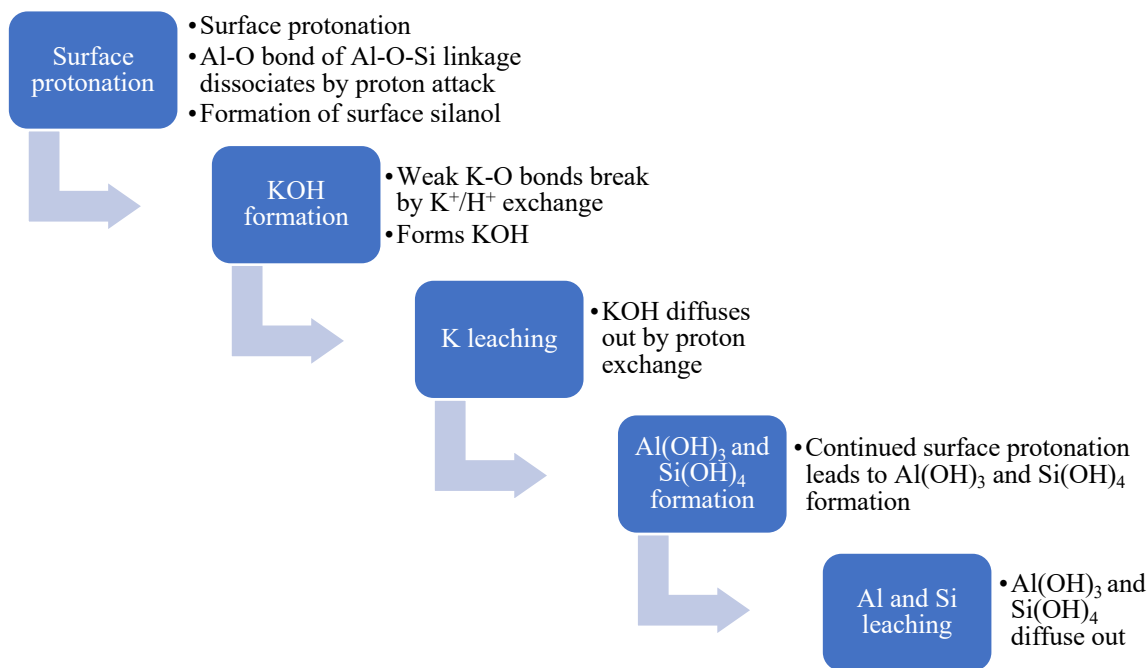


Figure 8. Schematic summary of the sequence of events that lead to leaching of cations from illite to surrounding water, obtained from ReaxFF simulations

Figure 6(a) shows the final step in the formation of a $\text{Si}(\text{OH})_4$ molecule by dissociation of the Al-O group and proton addition to the residual $\text{Si}(\text{OH})_3^+$ radical. A nascent $\text{Si}(\text{OH})_4$ molecule thus formed near the surface as shown in Fig. 6(b) diffuses into the fluid by a combined reactive/non-reactive diffusion shown in Fig.6(c). Likewise, Fig. 7(a) and (b) show the final two steps in the formation of $\text{Al}(\text{OH})_3$ molecule. In Fig. 7(a), an Al-O group with an unbonded O is neutralized by a proton as it passes to a configuration in Fig. 7(b), where the Al-O bond stretches and breaks leaving an undercoordinated Al, which binds with a free hydroxyl radical to form an $\text{Al}(\text{OH})_3$ molecule as shown in Fig. 7(c). In our simulations, we also find that Si leaches out earlier than Al, which may seem counterintuitive when the valency of Al (3+) and Si (4+) cations are

compared. Nevertheless, this trend can be justified as Si gets hydrated before Al because surface proton addition prefers the formation of silanol groups. Al seems to unbind from its tetragonal state and get triply hydrated to $\text{Al}(\text{OH})_3$ at the surface, at a slightly later stage, eventually dissolving into water. A similar Al/Si concentration ratio (< 1) was also observed by Smith et al.[51] who studied the dissolution of illite in water at elevated temperatures (100-280°C) and varying pH (3-9) values via dissolution experiments. A graphical summary the sequence of events leading to surface protonation, leaching of K, Al and Si structural atoms in our simulations, are given in Fig. 8, which explains the experimental results presented in Table 2. Given that ReaxFF can qualitatively predict the chemistry of leaching, now we utilize the MD data to probe into the kinetics of leaching.

3.3. Leaching kinetics

Next we predict the kinetics of mineral dissolution, a rather complex and long-timescale event by leveraging the early stage reaction events observed in MD simulations. If the surface reaction mechanism and energetics are accurately captured, then it is safe to assume that the early stage reaction kinetics is accurately captured by the forcefield. Based on this assumption, we try to assess if early-stage surface reaction kinetics be used as a surrogate model for long-timescale leaching events, by comparing the reaction kinetics obtained from MD simulations with the experimental data.

3.3.1. Evaluation of solute concentrations

Since a direct numerical comparison of the saturated cation concentration between simulation and experiments is not trivial because the rock is a mixture of minerals, we first thoroughly

characterize the rock to quantify the masses of different minerals. A chemical and modal analysis of the rock was also performed, and the results are provided in Table 3. Following this, we assume an equal reactivity to all the minerals (listed in Table 3) with water and attributed Si and Al to the minerals proportional to their weight ratio in the unreacted rock sample. For instance, the sources of Si are all the minerals except calcite and pyrite and the sources of Al are illite, kaolinite, chlorite, and albite. Based on the initial mass fraction of different clay minerals in the rocks and assuming that they leach out cations proportional to their mass fractions, the contributions from illite can be easily evaluated. The only source of K is illite, and hence, a direct numerical comparison between simulation and experiment is possible.

Table 3. Mineralogy of rock used in the experiment[21]

Mineral	wt %
Quartz	33.2
Silica (amorphous)	33.2
Calcite	20.1
Illite	6.3
Kaolinite	1.4
Chlorite	0.7
Albite	4.8
Pyrite	1.0

Based on the percent weight of illite in the unreacted rock, using molar masses of the minerals, the contribution to leached cations is evaluated. The contributions are: Si = 5.27%, Al = 53.33 %, K = 100%. The leached cation concentration reported in Herz-Thyhsen et al.[21] as: Si = 5.65×10^{-5} mol, Al = 5.3×10^{-7} mol, K = 4×10^{-4} mol respectively. Hence the final concentration of cations contributed by illite can be evaluated as: Si = 9.9×10^{-3} mmol/kg, Al = 9.36×10^{-4} mmol/kg, K = 1.94 mmol/kg.

The leached cation concentration from MD simulation is calculated from the mass (or number) density of cations in a region outside an interfacial region. An interfacial region is defined based on Gibbs dividing plane at z location z_G given by[52]:

$$\int_{-\infty}^{z_G} (\rho(z) - \rho_1) \cdot dz = - \int_{z_G}^{\infty} (\rho(z) - \rho_2) \cdot dz, \quad (1)$$

where $\rho(z)$ is the density of silicon atoms at spatial location z , ρ_1 and ρ_2 are densities of silicon in bulk illite and bulk water respectively, $-\infty$ and ∞ are the spatial locations where random ρ distribution is observed. For our case, this can be in the bulk illite and bulk water regions, respectively. Silicon atoms outside the interfacial region are considered to be leached silicon atoms.

3.3.2. Early stage surface reaction kinetics

Figure 9 (a)-(c) shows the number of leached ions as a function of time, evaluated using Eq. 1. We limited our simulation time to 400 ps, because at 3000 K, the structure tends to distort excessively beyond 400 ps that the simulations may not be representative of a crystalline illite phase. Based on the leached atom count, assuming a zero-order reaction kinetics, we fitted a rate equation:

$$k = \frac{\partial c}{\partial t}. \quad (2)$$

Here k is the rate constant, c is the solute concentration, and t is time. We then plotted the $\log(k)$ v/s $1/T$ curve as shown in Fig. 9(d) and extrapolated to experimental temperature of 488 K to estimate $k_{488 K}$.

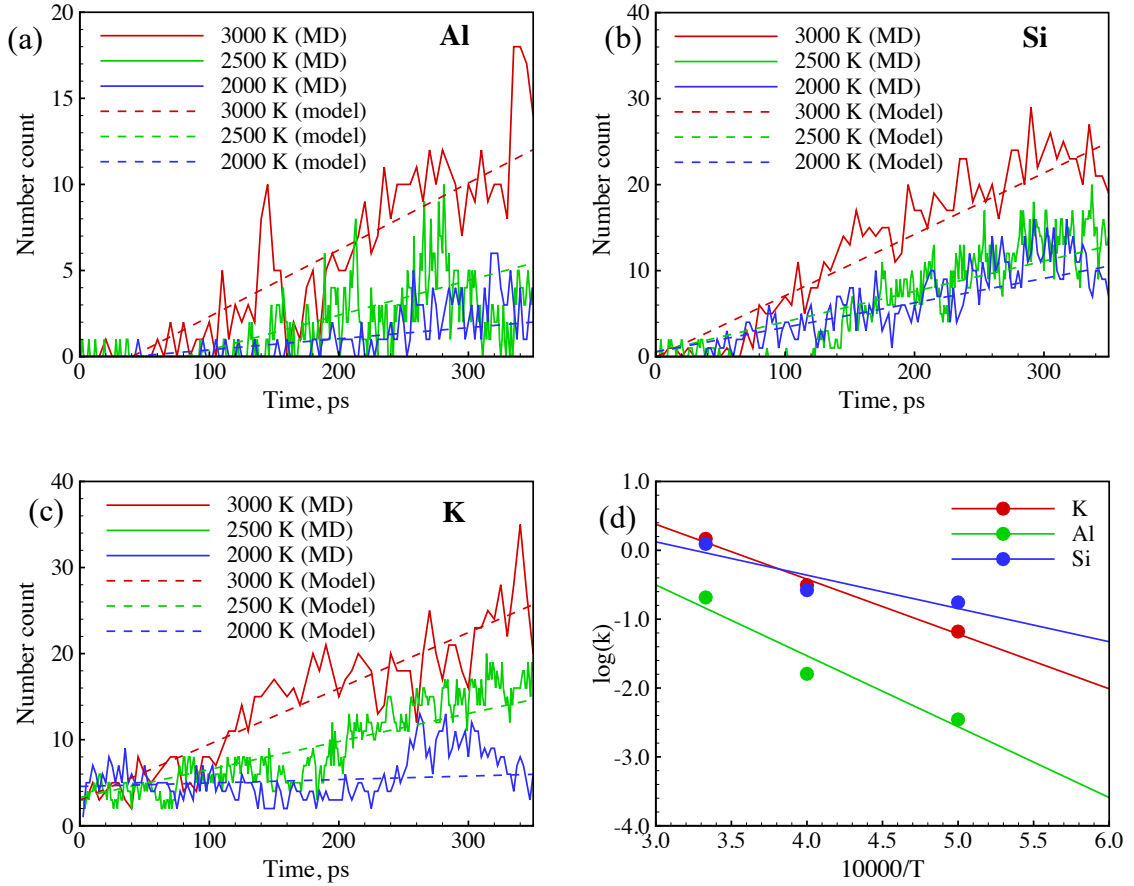


Figure 9. Early stage kinetic and rate constants. Number of leached atoms of a) Al, b) Si, and c) K at $T = 2000$ K, 2500 K, 3000 K. d) $\log(k)$ v/s $1/T$ equation fitted rate constants obtained by approximating a zero-order rate equation to data from (a), (b), and (c).

Using the calculated $k_{488 K}$ and equilibrium solute concentration obtained from experiments, the timescale of saturation using the equation was estimated from the equation:

$$c(t) = c_{sat}(1 - \exp(-k_{488 K} \cdot t)). \quad (3)$$

Here $c(t)$ is the solute concentration at time t , c_{sat} is the saturated solute concentration obtained from experiments. A similar approach based on reactive MD simulations can be found elsewhere.[53] Our model predictions are shown in Fig. 10(a) and the actual experimental

measurements are shown in Fig. 10(b). As can be seen from Fig.10, there is 8-9 orders of magnitude difference in the kinetics predicted by MD-derived kinetics model.

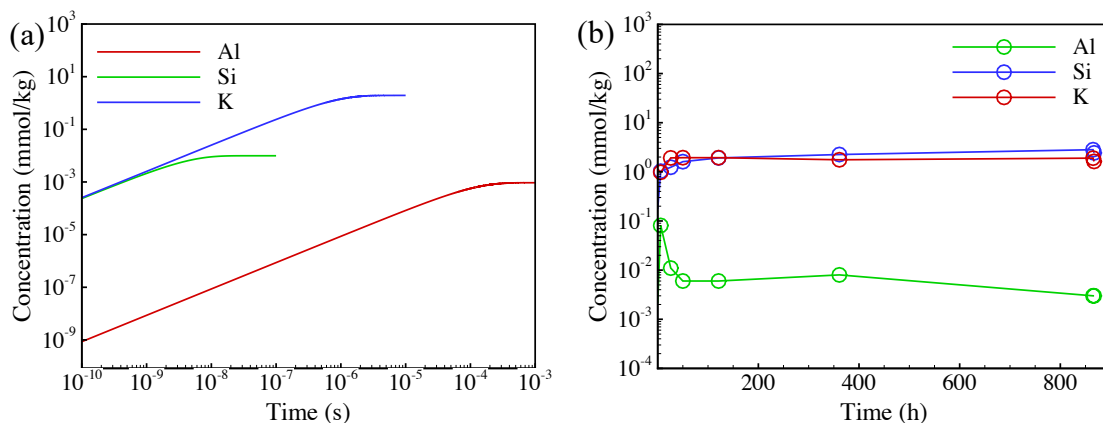


Figure 10. Plots showing the development of leached ion concentration in solution from model and experiments over time. a) Model predictions using $k_{T=488\text{ K}}$ and equilibrium solute concentration (obtained from experiments) and b) Solute concentrations measured using hydrothermal experiments.

We attribute this large disparity to several factors. Firstly, structural disruption and temperature acceleration create disproportionately large number of leached atoms within a small timescale of 400 ps. This can lead to an overprediction of reaction kinetics, and subsequently, underprediction of reaction time scales. Secondly, for extrapolating to 488 K, strictly speaking, illite should have the same crystalline structure at higher temperatures as well, which may not be the case here because at $T > 2000$ K, structure deviates from a perfect crystal (discussed in detail in section 3.3). Thirdly, early stage kinetics may not be a good surrogate model for leaching kinetics because it ignores contribution from solute reprecipitation and diffusion because of the limited timescales. In our simulations, we did not observe any reprecipitation events. For a fair comparison, either

experiments must be carried at higher temperatures or simulations must be conducted at lower temperatures. But both these approaches have practical difficulties. While experimental temperatures in the range 673-873 K have been reported in the literature, to our knowledge, no hydrothermal experiments at $T > 873$ K have been reported. Likewise, in low temperature simulations ($T < 1500$ K), we did not observe any reactive events that leads to leaching of ions because of the large energy barriers to bond dissociation. These results reveal the computational limitations of fully atomistic ReaxFF/MD implementation to model kinetics of leaching from crystalline materials. However, this may not be true for amorphous materials because the structure is disordered throughout the simulation and experiments, which creates avenues for easier diffusion and dissolution of counterions.[35]

3.4. Leaching and temperature-induced structural modifications to illite over time

Finally, we analyzed the structural modifications to illite crystal caused by leaching events and high temperatures. For this, we captured images of the illite structure before and after the dissolution process. Figure 11 shows the initial (unreacted rock) and final (after reaction) images of the illite surface obtained from hydrothermal experiments. Comparing Fig.11(a) and (b), the surface illite fibers have smoothed due to dissolution; an initial cube surface with protruding illite fibers have now pitted and dissolved. From Fig.11(c), when the interior surface is observed, much of the illite fibers have now been lost to the surrounding water due to diffusion of interior cations, while the fundamental Al-O-Si skeleton likely remains intact. Hence, it is quite evident that there is a significant structural transformation on illite surface.

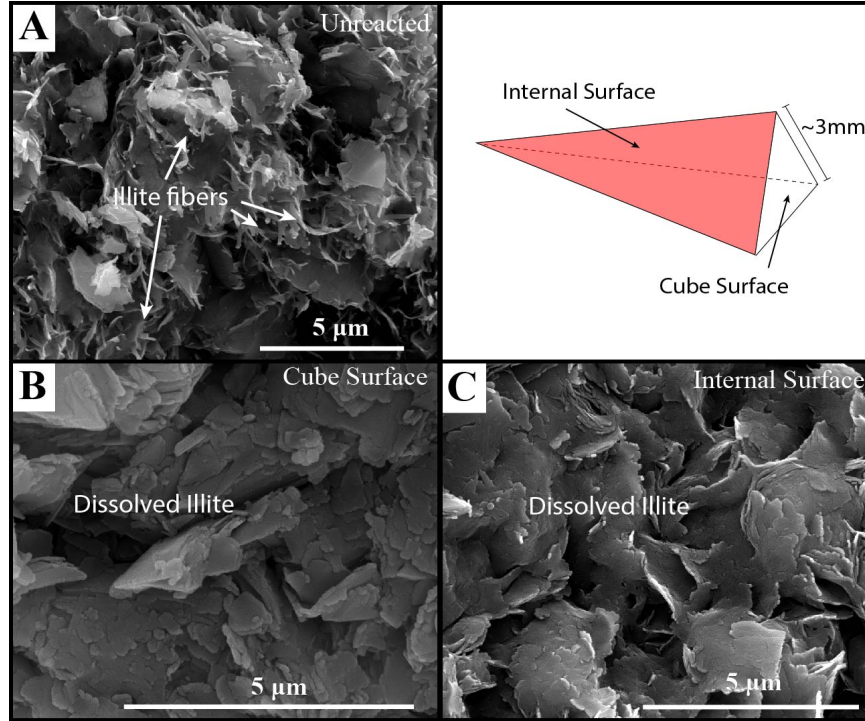


Figure 11. Visual comparison of images before and after dissolution from the hydrothermal experiments. a) Unreacted illite fibers, b) dissolved illite exterior (cube surface as depicted in the image on the top right corner), and c) dissolved illite interior[21].

This could be due to mineral dissolution and/or elevated temperatures. To investigate this phenomena, we first study the structural deformation to a single illite layer in the absence of water caused independently by temperature and leaching. To simulate the leaching-induced structural changes, Al and Si atoms are deliberately removed randomly from the structure and the system is equilibrated at room temperature for 250 ps. Figure 12 compares the effects of temperature, Al leaching, Si leaching, and temperature on the pairwise radial distribution function, ($g(r)$) of Al-Al and Si-Si interactions, representative of the structural ordering. As can be seen in the Fig. 12(a) and (b), $g(r)_{Al-Al}$ and $g(r)_{Si-Si}$ show gradually reducing heights of first three nearest neighbor interactions as the percentage of leached atoms are increased from 1 to 30%. It also suggests that

>20% leaching is required to induce a structural disorder to the surface layer. From Fig. 12(c) and (d), it is can be seen that an elevated temperature of 488 K does not distort the structure significantly; all the major peaks are retained in the first 250 ps of simulation indicating that the long-range order is not affected.

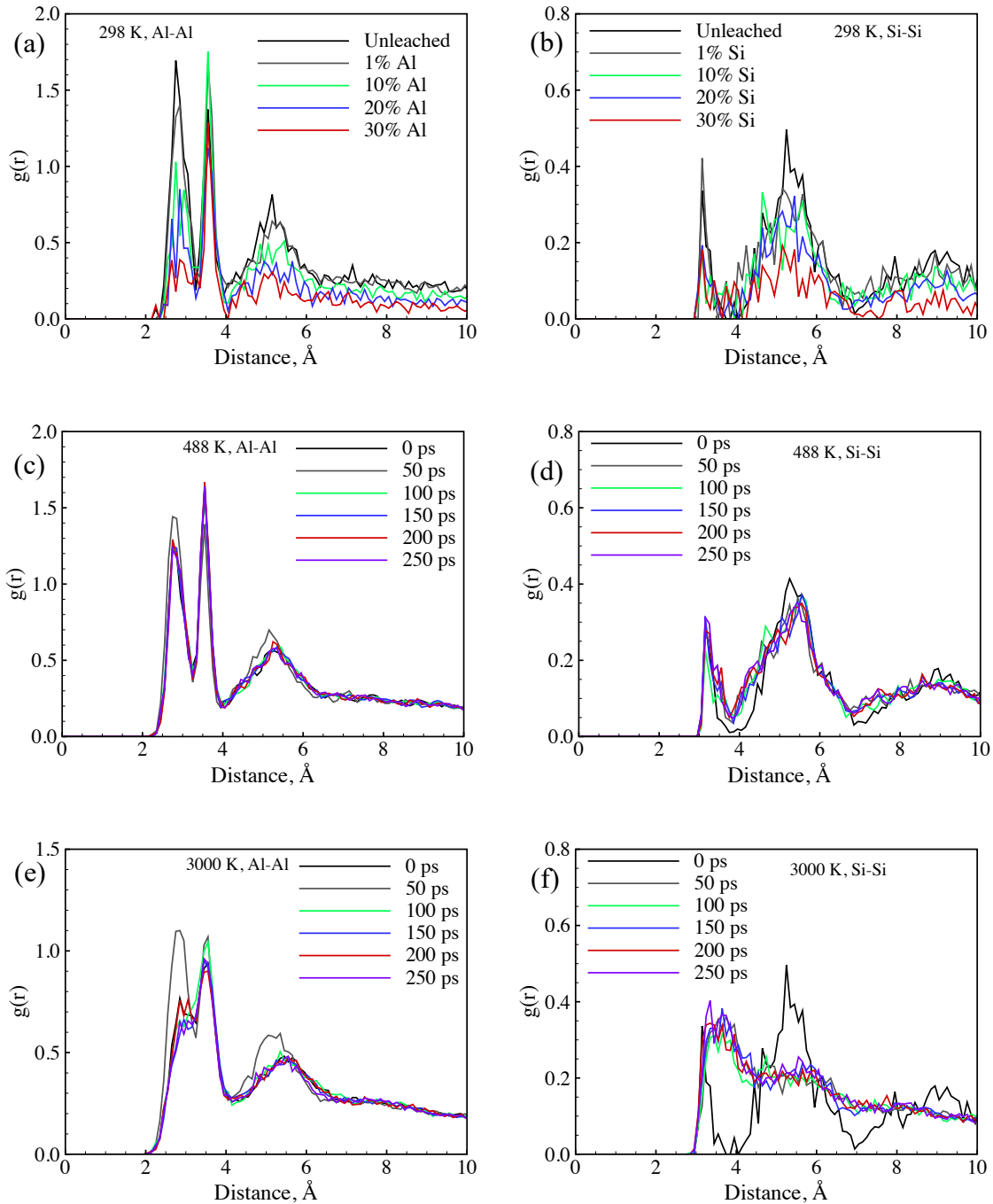


Figure 12. Radial density function of Al-Al and Si-Si interactions for a single layer aluminosilicate sheet a) $g(r)_{Al-Al}$ for different amounts of Al atoms removed from the lattice, b) $g(r)_{Si-Si}$ for different amounts of Si atoms removed from the lattice, c) $g(r)_{Al-Al}$ at $T = 488$ K, d) $g(r)_{Si-Si}$ at $T = 488$ K, e) $g(r)_{Al-Al}$ at $T = 3000$ K, f) $g(r)_{Si-Si}$ at $T = 3000$ K

Furthermore, we also studied the effect of simulation temperature of 3000 K on an aluminosilicate sheet, as shown in Fig. 12(e) and (f). $g(r)_{Al-Al}$ shows gradually diminishing first-neighbor ordering while $g(r)_{Si-Si}$ shows that the first-neighbor peaks broaden, with no signs of long-range order, suggesting that the system has lost its crystallinity at $T = 3000$ K. Hence, simulation temperature has a major role in deciding the structural stability of the solid, which in turn decides the number of leached atoms. This poses an open question on whether we can observe interior cations leaching out at room temperatures in ReaxFF/MD simulations given sufficient simulation time or if this is merely an artefact of the high temperatures that modifies the illite structure causing disorderliness,[54] which opens up avenues for species diffusion. To thoroughly investigate this, one could use accelerated MD techniques like metadynamics,[55] parallel tempering,[56] parallel replica dynamics[57] and hyperdynamics[58] at lower temperatures to boost infrequent predetermined reactions that have high energy barriers and are less probable at low temperatures. Since the focus of the present study is to identify the chemical pathway of cation leaching, a suggested direction for future studies is to implement an appropriate accelerated MD technique that speeds up the kinetics of these reactions at low temperatures to boost the leaching events.

4. Conclusions

We have elucidated the chemical mechanism of leaching of cations from a clay mineral/fluid interfacial system by means of reactive molecular dynamics and hydrothermal experiments. ReaxFF methodology was used to simulate chemistry-induced dissolution and structural transformations in illite when in contact with water. Hydrothermal experiments using rocking furnace-pressure vessel assembly was conducted on rock cut from core of the Wall Creek Member of the Frontier Formation from the Powder River Basin, Wyoming. First, we utilized the ReaxFF capability to elucidate possible chemical reaction mechanisms that lead to the leaching of K, Al, and Si. It was found that water, when placed in contact with an illite surface, supplies protons that bind with the non-bridging oxygen on Al-O-Si linkage and cleaves the Al-O bonds, forming silanol group at the surface. The terminal Al transitions from octahedral to tetrahedral Al and the residue OH⁻ remains in the fluid. When protons are supplied to illite, the counterion K-O bonds become weaker and K⁺ cations tend to diffuse freely in the crystal. The K⁺ cations that reach the surface binds with OH⁻ species to neutralize the excess negative charge to form a KOH molecule. KOH molecule later diffuses out to bulk water by proton exchange mechanism. Continued protonation results in breaking more Al-O and Si-O bonds and the formation of Al(OH)₃ and Si(OH)₄ molecules at the surface. Diffusion of protons to the interior of crystal helps in breaking more Al-O-Si linkages and freeing more cations. The Al³⁺ and Si⁴⁺ cations also leach out to the bulk fluid non-reactively or reactively, but this is a comparatively slow process. We also observe a similar trend in the dissolution of Al and Si cations in our experimental measurements. Our comparison of leaching kinetics obtained from simulations and experiments show significant disparity, suggesting that early stage surface reaction kinetics may be overpredicting the leaching rates. Furthermore, upon analyzing the effect of leaching on structural distortion, a notable distortion to

an initially crystalline illite structure is observed for leaching of >20% atoms. In summary, ReaxFF approach is demonstrated to be a reliable tool to understand the reaction mechanisms leading to cation leaching and leaching-driven structural transformations in solid-fluid interfacial systems but needs further refinements for capturing leaching kinetics accurately.

Acknowledgements

We acknowledge funding support from the Multi-Scale Fluid-Solid Interactions in Architected and Natural Materials (MUSE) Center, an Energy Frontier Research Center funded by the U.S. Department of Energy (DOE), Office of Science, Basic Energy Sciences. Herz-Thyhsen, Dewey and Kaszuba acknowledge and thank the Office of Academic Affairs for partial support of this research through an Energy Graduate Assistantship award. We also thank Paul Lawless and Helis Oil & Gas for generously donating core and invaluable knowledge. We thank Susan Swapp and TylerBrown for assistance with SEM and XRD analyses. We thank Virginia Marcon, Alexa Socianu, Steve Levesque, and Jeff Martin for support in the laboratory. Kaszuba's work was in part supported by the University of Wyoming School of Energy Resources and a Nielson Energy Fellowship.

References

- [1] D.W. Johnson, D.D. Richter, H. Van Miegroet, D.W. Cole, Contributions of acid deposition and natural processes to cation leaching from forest soils: a review, *J. Air Pollut. Control Assoc.* 33 (1983) 1036–1041.
- [2] D. Mishra, G.R. Chaudhury, D.J. Kim, J.G. Ahn, Recovery of metal values from spent petroleum catalyst using leaching-solvent extraction technique, *Hydrometallurgy*. 101

- (2010) 35–40.
- [3] M. Li, C. Wei, G. Fan, C. Li, Z. Deng, X. Li, Extraction of vanadium from black shale using pressure acid leaching, *Hydrometallurgy*. 98 (2009) 308–313.
- [4] M.-T. Li, W.E.I. Chang, F.A.N. Gang, C.-X. Li, Z.-G. Deng, X.-B. Li, Pressure acid leaching of black shale for extraction of vanadium, *Trans. Nonferrous Met. Soc. China*. 20 (2010) s112–s117.
- [5] C. Abbruzzese, P. Fornari, R. Massidda, F. Vegliò, S. Ubaldini, Thiosulphate leaching for gold hydrometallurgy, *Hydrometallurgy*. 39 (1995) 265–276.
- [6] M.K. Jha, V. Kumar, R.J. Singh, Review of hydrometallurgical recovery of zinc from industrial wastes, *Resour. Conserv. Recycl.* 33 (2001) 1–22.
- [7] P. Baláž, M. Achimovičová, Mechano-chemical leaching in hydrometallurgy of complex sulphides, *Hydrometallurgy*. 84 (2006) 60–68.
- [8] L. Li, J. Ge, R. Chen, F. Wu, S. Chen, X. Zhang, Environmental friendly leaching reagent for cobalt and lithium recovery from spent lithium-ion batteries, *Waste Manag.* 30 (2010) 2615–2621.
- [9] M.K. Jha, A. Kumari, A.K. Jha, V. Kumar, J. Hait, B.D. Pandey, Recovery of lithium and cobalt from waste lithium ion batteries of mobile phone, *Waste Manag.* 33 (2013) 1890–1897.
- [10] G. Heckrath, P.C. Brookes, P.R. Poulton, K.W.T. Goulding, Phosphorus leaching from soils containing different phosphorus concentrations in the Broadbalk experiment, *J. Environ. Qual.* 24 (1995) 904–910.
- [11] S. Pugesgaard, K. Schelde, S.U. Larsen, P.E. Lærke, U. Jørgensen, Comparing annual and perennial crops for bioenergy production–influence on nitrate leaching and energy

- balance, *Gcb Bioenergy*. 7 (2015) 1136–1149.
- [12] G. Goodlass, M. Green, B. Hilton, S. McDonough, Nitrate leaching from short-rotation coppice, *Soil Use Manag.* 23 (2007) 178–184.
- [13] V. Marcon, C. Joseph, K.E. Carter, S.W. Hedges, C.L. Lopano, G.D. Guthrie, J.A. Hakala, Experimental insights into geochemical changes in hydraulically fractured Marcellus Shale, *Appl. Geochemistry*. 76 (2017) 36–50.
- [14] A.L. Harrison, A.D. Jew, M.K. Dustin, D.L. Thomas, C.M. Joe-Wong, J.R. Bargar, N. Johnson, G.E. Brown Jr, K. Maher, Element release and reaction-induced porosity alteration during shale-hydraulic fracturing fluid interactions, *Appl. Geochemistry*. 82 (2017) 47–62.
- [15] J. Xiao, J. Li, Z. Xu, Novel approach for in situ recovery of lithium carbonate from spent lithium ion batteries using vacuum metallurgy, *Environ. Sci. Technol.* 51 (2017) 11960–11966.
- [16] L. Sinclair, J. Thompson, In situ leaching of copper: Challenges and future prospects, *Hydrometallurgy*. 157 (2015) 306–324.
- [17] G.G. Hunkin, T.P. Fife, J.R. Stano, In situ carbonate leaching and recovery of uranium from ore deposits, (1979).
- [18] A.R. Hind, S.K. Bhargava, S.C. Grocott, The surface chemistry of Bayer process solids: a review, *Colloids Surfaces A Physicochem. Eng. Asp.* 146 (1999) 359–374.
- [19] A. Tessier, P.G.C. Campbell, M. Bisson, Sequential extraction procedure for the speciation of particulate trace metals, *Anal. Chem.* 51 (1979) 844–851.
- [20] B. Velde, *Clay minerals*, (1985).
- [21] R.J. Herz-Thyhsen, J.P. Kaszuba, J.C. Dewey, Mineral dissolution and precipitation in

- low-permeability sandstone surrounding fractures induced by hydraulic fracturing, *Energy & Fuels*. In Review (2019).
- [22] E. Ferrage, B.A. Sakharov, L.J. Michot, A. Delville, A. Bauer, B. Lanson, S. Grangeon, G. Frapper, M. Jiménez-Ruiz, G.J. Cuello, Hydration properties and interlayer organization of water and ions in synthetic Na-smectite with tetrahedral layer charge. Part 2. Toward a precise coupling between molecular simulations and diffraction data, *J. Phys. Chem. C*. 115 (2011) 1867–1881.
- [23] A. Botan, B. Rotenberg, V. Marry, P. Turq, B. Noetinger, Carbon dioxide in montmorillonite clay hydrates: thermodynamics, structure, and transport from molecular simulation, *J. Phys. Chem. C*. 114 (2010) 14962–14969.
- [24] Y. Yu, X. Yang, Molecular simulation of swelling and interlayer structure for organoclay in supercritical CO₂, *Phys. Chem. Chem. Phys.* 13 (2011) 282–290.
- [25] J.L. Suter, P. V Coveney, H.C. Greenwell, M.-A. Thyveetil, Large-scale molecular dynamics study of montmorillonite clay: emergence of undulatory fluctuations and determination of material properties, *J. Phys. Chem. C*. 111 (2007) 8248–8259.
- [26] M.A. Mazo, L.I. Manevitch, E.B. Gusarova, M.Y. Shamaev, A.A. Berlin, N.K. Balabaev, G.C. Rutledge, Molecular dynamics simulation of thermomechanical properties of montmorillonite crystal. 1. Isolated clay nanoplate, *J. Phys. Chem. B*. 112 (2008) 2964–2969.
- [27] L. Aristilde, C. Marichal, J. Miehe-Brendle, B. Lanson, L. Charlet, Interactions of oxytetracycline with a smectite clay: a spectroscopic study with molecular simulations, *Environ. Sci. Technol.* 44 (2010) 7839–7845.
- [28] V.K. Voora, W.A. Al-Saidi, K.D. Jordan, Density functional theory study of pyrophyllite

- and M-montmorillonites (M= Li, Na, K, Mg, and Ca): Role of dispersion interactions, *J. Phys. Chem. A.* 115 (2011) 9695–9703.
- [29] J.P. Larentzos, J.A. Greathouse, R.T. Cygan, An ab initio and classical molecular dynamics investigation of the structural and vibrational properties of talc and pyrophyllite, *J. Phys. Chem. C.* 111 (2007) 12752–12759.
- [30] A.C.T. Van Duin, S. Dasgupta, F. Lorant, W.A. Goddard, ReaxFF: a reactive force field for hydrocarbons, *J. Phys. Chem. A.* 105 (2001) 9396–9409.
- [31] K. Chenoweth, A.C.T. Van Duin, W.A. Goddard, ReaxFF reactive force field for molecular dynamics simulations of hydrocarbon oxidation, *J. Phys. Chem. A.* 112 (2008) 1040–1053.
- [32] J. Yeon, A.C.T. Van Duin, ReaxFF molecular dynamics simulations of hydroxylation kinetics for amorphous and nano-silica structure, and its relations with atomic strain energy, *J. Phys. Chem. C.* 120 (2015) 305–317.
- [33] M.C. Pitman, A.C.T. Van Duin, Dynamics of confined reactive water in smectite clay–zeolite composites, *J. Am. Chem. Soc.* 134 (2012) 3042–3053.
- [34] M. Fedkin, Y.K. Shin, N. Dasgupta, J. Yeon, W. Zhang, D. Van Duin, A.C.T. van Duin, K. Mori, A. Fujiwara, M. Machida, Development of the ReaxFF Methodology for Electrolyte-Water Systems, *J. Phys. Chem. A.* (2019).
- [35] S.H. Hahn, A.C.T. van Duin, Surface Reactivity and Leaching of a Sodium Silicate Glass Under Aqueous Environment: A ReaxFF Molecular Dynamics Study, *J. Phys. Chem. C.* (2019).
- [36] M.G. Muraleedharan, H. Asgar, S. Mohammed, G. Gadikota, A.C.T. van Duin, Elucidating Thermally Induced Structural and Chemical Transformations in Kaolinite

- using Reactive Molecular Dynamics Simulations and X-Ray Scattering Measurements, *Chem. Mater.* (2019).
- [37] S.H. Hahn, J. Rimsza, L. Criscenti, W. Sun, L. Deng, J. Du, T. Liang, S.B. Sinnott, A.C.T. Van Duin, Development of a ReaxFF reactive force field for NaSiO_x/water systems and its application to sodium and proton self-diffusion, *J. Phys. Chem. C.* 122 (2018) 19613–19624.
- [38] W.J. Mortier, S.K. Ghosh, S. Shankar, Electronegativity-equalization method for the calculation of atomic charges in molecules, *J. Am. Chem. Soc.* 108 (1986) 4315–4320.
- [39] E.J. Baerends, T. Ziegler, A.J. Atkins, J. Autschbach, D. Bashford, O. Baseggio, A. Bérces, F.M. Bickelhaupt, C. Bo, P.M. Boerritger, L. Cavallo, C. Daul, D.P. Chong, D. V Chulhai, L. Deng, R.M. Dickson, J.M. Dieterich, D.E. Ellis, M. van Faassen, A. Ghysels, A. Giammona, S.J.A. van Gisbergen, A. Goetz, A.W. Götz, S. Gusarov, F.E. Harris, P. van den Hoek, Z. Hu, C.R. Jacob, H. Jacobsen, L. Jensen, L. Joubert, J.W. Kaminski, G. van Kessel, C. König, F. Kootstra, A. Kovalenko, M. Krykunov, E. van Lenthe, D.A. McCormack, A. Michalak, M. Mitoraj, S.M. Morton, J. Neugebauer, V.P. Nicu, L. Noodleman, V.P. Osinga, S. Patchkovskii, M. Pavanello, C.A. Peeples, P.H.T. Philipsen, D. Post, C.C. Pye, H. Ramanantoanina, P. Ramos, W. Ravenek, J.I. Rodríguez, P. Ros, R. Rüger, P.R.T. Schipper, D. Schlüns, H. van Schoot, G. Schreckenbach, J.S. Seldenthuis, M. Seth, J.G. Snijders, M. Solà, S. M., M. Swart, D. Swerhone, G. te Velde, V. Tognetti, P. Vernooijs, L. Versluis, L. Visscher, O. Visser, F. Wang, T.A. Wesolowski, E.M. van Wezenbeek, G. Wiesenekker, S.K. Wolff, T.K. Woo, A.L. Yakovlev, ADF2017, SCM, Theoretical Chemistry, Vrije Universiteit, Amsterdam, The Netherlands, <https://www.scm.com>, (n.d.).

- [40] M.P. Allen, D.J. Tildesley, *Computer simulation of liquids*, Oxford university press, 2017.
- [41] R.J. Herz-Thyhsen, J.P. Kaszuba, J.C. Dewey, *Dissolution of Minerals and Precipitation of an Aluminosilicate Phase during Experimentally Simulated Hydraulic Fracturing of a Mudstone and a Tight Sandstone in the Powder River Basin, WY*, *Energy & Fuels*. 33 (2019) 3947–3956.
- [42] J.P. Kaszuba, D.R. Janecky, M.G. Snow, *Carbon dioxide reaction processes in a model brine aquifer at 200 C and 200 bars: implications for geologic sequestration of carbon*, *Appl. Geochemistry*. 18 (2003) 1065–1080.
- [43] W.E. Seyfried Jr, D.R. Janecky, M.E. Berndt, *Rocking autoclaves for hydrothermal experiments II. The flexible reaction-cell system*, *Hydrothermal Exp. Tech*. 23 (1987).
- [44] D. O'Malley, S. Karra, R.P. Currier, N. Makedonska, J.D. Hyman, H.S. Viswanathan, *Where does water go during hydraulic fracturing?*, *Groundwater*. 54 (2016) 488–497.
- [45] P.R. Haddad, P.E. Jackson, *Ion chromatography*, Elsevier, 1990.
- [46] E.W.D. Huffman jr, *Performance of a new automatic carbon dioxide coulometer*, *Microchem. J*. 22 (1977) 567–573.
- [47] H. Van Olphen, *Thermodynamics of interlayer adsorption of water in clays. I.—Sodium vermiculite*, *J. Colloid Sci*. 20 (1965) 822–837.
- [48] A. Zen, L.M. Roch, S.J. Cox, X.L. Hu, S. Sorella, D. Alfè, A. Michaelides, *Toward accurate adsorption energetics on clay surfaces*, *J. Phys. Chem. C*. 120 (2016) 26402–26413.
- [49] M.G. Muraleedharan, D.S. Sundaram, A. Henry, V. Yang, *Thermal conductivity calculation of nano-suspensions using Green-Kubo relations with reduced artificial correlations*, *J. Phys. Condens. Matter*. 29 (2017). doi:10.1088/1361-648X/aa5f08.

- [50] D. Sheppard, R. Terrell, G. Henkelman, Optimization methods for finding minimum energy paths, *J. Chem. Phys.* 128 (2008) 134106.
- [51] M.M. Smith, Z. Dai, S.A. Carroll, Illite dissolution kinetics from 100 to 280° C and pH 3 to 9, *Geochim. Cosmochim. Acta.* 209 (2017) 9–23.
- [52] B.V.P. SOKHAN, D.J. Tildesley, The free surface of water: molecular orientation, surface potential and nonlinear susceptibility, *Mol. Phys.* 92 (1997) 625–640.
- [53] T. Du, H. Li, Q. Zhou, Z. Wang, G. Sant, J. V Ryan, M. Bauchy, Chemical composition of calcium-silicate-hydrate gels: Competition between kinetics and thermodynamics, *Phys. Rev. Mater.* 3 (2019) 65603.
- [54] F. DeAngelis, M.G. Muraleedharan, J. Moon, H.R. Seyf, A.J. Minnich, A.J.H. McGaughey, A. Henry, Thermal Transport in Disordered Materials, *Nanoscale Microscale Thermophys. Eng.* (2018) 1–36.
- [55] K.M. Bal, E.C. Neyts, Direct observation of realistic-temperature fuel combustion mechanisms in atomistic simulations, *Chem. Sci.* 7 (2016) 5280–5286.
- [56] L. Atmani, C. Bichara, R.J.-M. Pellenq, H. Van Damme, A.C.T. van Duin, Z. Raza, L.A. Truflandier, A. Obliger, P.G. Kralert, F.J. Ulm, From cellulose to kerogen: molecular simulation of a geological process, *Chem. Sci.* 8 (2017) 8325–8335.
- [57] A.F. Voter, Parallel replica method for dynamics of infrequent events, *Phys. Rev. B.* 57 (1998) R13985.
- [58] A.F. Voter, Hyperdynamics: Accelerated molecular dynamics of infrequent events, *Phys. Rev. Lett.* 78 (1997) 3908.